

Photocatalysis

International Edition: DOI: 10.1002/anie.201914565
German Edition: DOI: 10.1002/ange.201914565

Electron Configuration Modulation of Nickel Single Atoms for Elevated Photocatalytic Hydrogen Evolution

Xixiong Jin, Rongyan Wang, Lingxia Zhang,* Rui Si,* Meng Shen, Min Wang, Jianjian Tian, and Jianlin Shi*

Abstract: The emerging metal single-atom catalyst has aroused extensive attention in multiple fields, such as clean energy, environmental protection, and biomedicine. Unfortunately, though it has been shown to be highly active, the origins of the activity of the single-atom sites remain unrevealed to date owing to the lack of deep insight on electronic level. Now, partially oxidized Ni single-atom sites were constructed in polymeric carbon nitride (CN), which elevates the photocatalytic performance by over 30-fold. The 3d orbital of the partially oxidized Ni single-atom sites is filled with unpaired d-electrons, which are ready to be excited under irradiation. Such an electron configuration results in elevated light response, conductivity, charge separation, and mobility of the photocatalyst concurrently, thus largely augmenting the photocatalytic performance.

Introduction

Photocatalytic hydrogen production from water splitting is expected to be a promising route to ensure sustainable green energy supply.^[1] Unfortunately, the lack of surface-active sites and the fast charge recombination of current photocatalysts are two of the main obstacles in further enhancing the photocatalytic performance. Recently, the emergence of single-atom cocatalysts has provided a new strategy to construct efficient surface active sites,^[2] overcoming the deficiencies of traditional metal nanoparticles, such as limited atom utilization and sluggish charge transfer.^[3] More importantly, the unsaturated coordination sites of isolated metal atoms offer a flexible electronic environment

to activate the catalyst and elevate its catalytic activity.^[4] However, most of the previous reports focused on the influence of local atom geometric configuration around center atoms on the photocatalytic performance; few emphasized the role of the electronic state of the metal single atoms in the course of photocatalytic reaction,^[5] or mentioned the fine modulation of the electron configuration of the single atoms. Intriguingly, recent studies on the behavior of d-electrons shed light on the modification of transition-metal single atoms. Yang et al. discovered that the delocalization of unpaired electron on Ni 3d_{x²-y²} orbital facilitates the charge transfer from Ni atom to adsorbed CO₂ molecules, lowering the energy barrier of CO₂ activation.^[5a] Lee et al. reported the reversible photoactivation of Cu single atoms on TiO₂, in which the Cu d-orbital electrons changed the valence state of Cu and activated the TiO₂ matrix, significantly enhancing the photocatalytic performance.^[2c] It has also been reported that the photocatalytic performance can be significantly improved by simply tuning the surface oxidation state of Ni nanoparticles, which most possibly results from the d-electron activation of transition metals.^[6] Keeping these in mind, we expect that it will be of high probability to achieve a further elevated catalytic activity by merely modulating the oxidation state of transition-metal single-atom sites, that is, activating the d-electrons of transition metal single atoms.

Herein we report a facile strategy to activate Ni single-atom sites by elaborately modulating the electron configuration of Ni atoms. Polymeric carbon nitride (CN) was chosen as the photocatalyst substrate owing to its unique N/C-coordinating network consisting of tri-s-triazine structure, forming stable binding sites for metal atoms.^[7] The Ni single-atom sites were constructed via a facile freezing-deposition method, in which bulky CN was successively ultrasonicated in NiCl₂ solution for 3 hours, and freeze-dried to guarantee the atomic level dispersion of Ni species (the obtained samples were named as CN-*x*Ni²⁺, where *x* is the atomic percentage of Ni in the samples). Subsequently, the powder was calcined in H₂, or O₂, or H₂ followed by O₂, producing photocatalysts accordingly denoted as CN-*x*Ni-H, CN-*x*Ni-O, and CN-*x*Ni-HO, respectively (see the Supporting Information, Experimental Procedures). Bulky CN calcined in H₂ or O₂ at 350 °C were also prepared as control samples denoted as CN-O and CN-H, respectively.

[*] X. Jin, Dr. R. Wang, Prof. L. Zhang, M. Shen, M. Wang, J. Tian, Prof. J. Shi
State Key Laboratory of High Performance Ceramics and Superfine Microstructure, Shanghai Institute of Ceramics
Chinese Academy of Sciences
1295 Dingxi Road, Shanghai 200050 (P. R. China)
and
Center of Materials Science and Optoelectronics Engineering
University of Chinese Academy of Sciences
19A Yuquan Road, Beijing 100049 (P. R. China)
E-mail: zhlingxia@mail.sic.ac.cn
jlshi@mail.sic.ac.cn
Prof. R. Si
Shanghai Synchrotron Radiation Facility, Zhangjiang Laboratory
239 Zhangheng Road, Shanghai 201204 (P. R. China)
E-mail: sirui@sinap.ac.cn

 Supporting information and the ORCID identification number(s) for the author(s) of this article can be found under:
 <https://doi.org/10.1002/anie.201914565>.

Results and Discussion

Structure Characterization

The morphology of the as-synthesized catalysts were carefully characterized. The two-dimensional (2D) sheet-like texture and functional groups of CN have been well-maintained after Ni deposition and calcination under different conditions. Meanwhile, no metallic Ni particles could be found on the surface of CN even at the Ni incorporation amount of 0.5 at%, corresponding to a mass percentage of 2.2 wt%, suggesting the homogeneous distribution of Ni atoms. The structural characterizations on the control samples of CN-O and CN-H exhibit that such treatments have brought negligible structural changes of CN network (Supporting Information, Figures S1–S4). The isolated bright spots of about 0.2 nm in average size observed in the high-angle annular dark-field scanning transmission electron microscopy (HAADF-STEM) image correspond to Ni atoms on CN (Figure 1a). The local coordination structure of Ni atoms on CN substrate was revealed by the phase-corrected Fourier transformation of Ni K-edge extended X-ray absorption fine structure spectroscopy (FT-EXAFS). The spectra of all samples exhibit only one single peak centered at about 2.0 Å, attributed to Ni-C/N bonding, while no Ni-Ni and Ni-O-Ni characteristic peaks can be identified at 2.5 Å (typical shell of Ni foil) and 2.9 Å (typical shell of Ni-O-Ni structure), respectively. These results show that Ni single atoms are only coordinated with C and N atoms and atomically dispersed on CN substrate (Figure 1b). The fitting results give the coordination number of circa 5 at 2.06 Å (Figure 1c; Supporting Information, Figure S5 and Table S1). It should be noted that the contribution from coordinated C and N atoms cannot be distinguished in extended X-ray absorption fine structure spectroscopy (EXAFS), due to the similar scattering factor between C and N. Accordingly, the position of the stabilized

Ni single atoms has been determined to be at the bottom of the five-membered rings of CN by density functional theory (DFT) calculation, where one Ni atom is bonded with four N atoms and one C atom (Figure 1d). These results clearly prove that Ni single-atom sites are stabilized in the framework of CN owing to the low electronegativity of the coordinated N and C atoms (Supporting Information, Figure S6) without compromising its crystal structure and polymeric framework, thus preserving the photo-responsive feature of the as-prepared photocatalyst.

Analysis of Chemical States of Ni Single-Atom Sites

The chemical states of Ni single-atom sites were finely tuned by adopting different calcination procedures. It should be noted that the pristine skeleton structure of CN has been well-maintained during Ni incorporation and calcination under different conditions (Supporting Information, Figures S1–S4). The X-ray absorption near-edge structure (XANES) profiles of the K-edge of Ni single atoms on CN after various calcination treatments, and in metallic Ni foil and NiO, are shown in Figure 2a. The average chemical valences of Ni single-atom sites were calculated from the linear combination fittings on XANES profiles (Supporting Information, Figure S5 and Table S1). It is exhibited that the chemical valence of Ni single-atom sites rises with the deepening oxidation, getting closer to that of Ni²⁺. The X-ray photoelectron spectroscopy (XPS) spectra of Ni single-atom sites are further deconvoluted to reveal their intermediate oxidation states (Figure 2b). For non-calcined sample CN-0.2Ni²⁺, the XPS spectrum only shows two spin-orbit doublets of Ni 2p with two shake-up satellites, characteristic of Ni²⁺. After calcination in different atmospheres, Ni single atoms in each sample exhibits unique valence state accordingly. Two new characteristic peaks at about 852 eV and about 869 eV attributed to Ni⁰ are found in the Ni 2p spectra of CN-0.2Ni-H and CN-0.2Ni-HO.^[6a] The percentage of Ni⁰ peak area decreases from 11.36% in CN-0.2Ni-H to 9.73% in CN-0.2Ni-HO, almost half of the percentage of Ni²⁺ peak area in CN-0.2Ni-HO (19.87%). Note that no peak of NiO is observed on these oxidized samples, indicating that such an oxidation process has only changed the coordination environment of Ni single-atom sites but no nickel oxide has been generated. This suggests that the oxidation states of the Ni single atoms can be precisely modulated into an intermediate oxidation state with a Ni²⁺/Ni⁰ ratio of about 2:1 via the calcinations in H₂ followed with O₂.

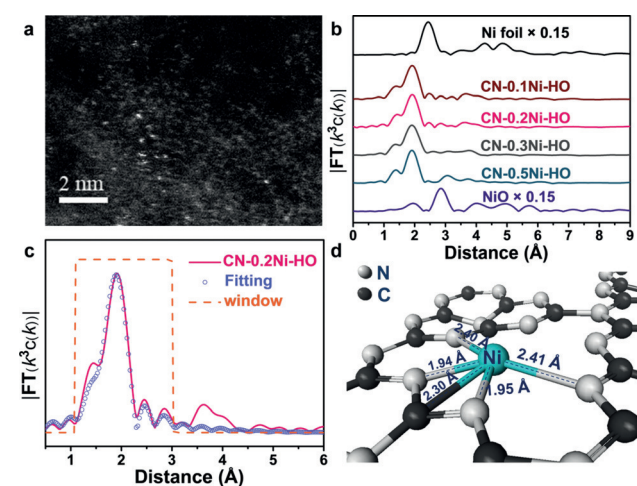


Figure 1. a) HAADF-STEM image of CN-0.5 Ni-HO. b) Ni K-edge FT-EXAFS spectra of Ni foil, Ni single-atom-coordinated CN with varied Ni contents from 0.1 to 0.5 at%, and NiO. c) Fitting results of FT-EXAFS for CN-0.2Ni-HO. d) Model of Ni single-atom site in CN. C black, N light gray, Ni green. The average bond length of Ni-C/N (2.20 Å) agrees well with the FT-EXAFS results.

Influences on the Electronic Configuration

Such partially oxidized Ni single-atom sites brought significant influences on the electronic configuration of the catalyst. Electron paramagnetic resonance (EPR) spectroscopy was employed to probe the unpaired electrons in the catalysts (Figure 2c). The characteristic peak centered at about 337 mT with a corresponding g-value of 2.0 originates from the C atoms in CN.^[8] Another g-value of 2.1 only

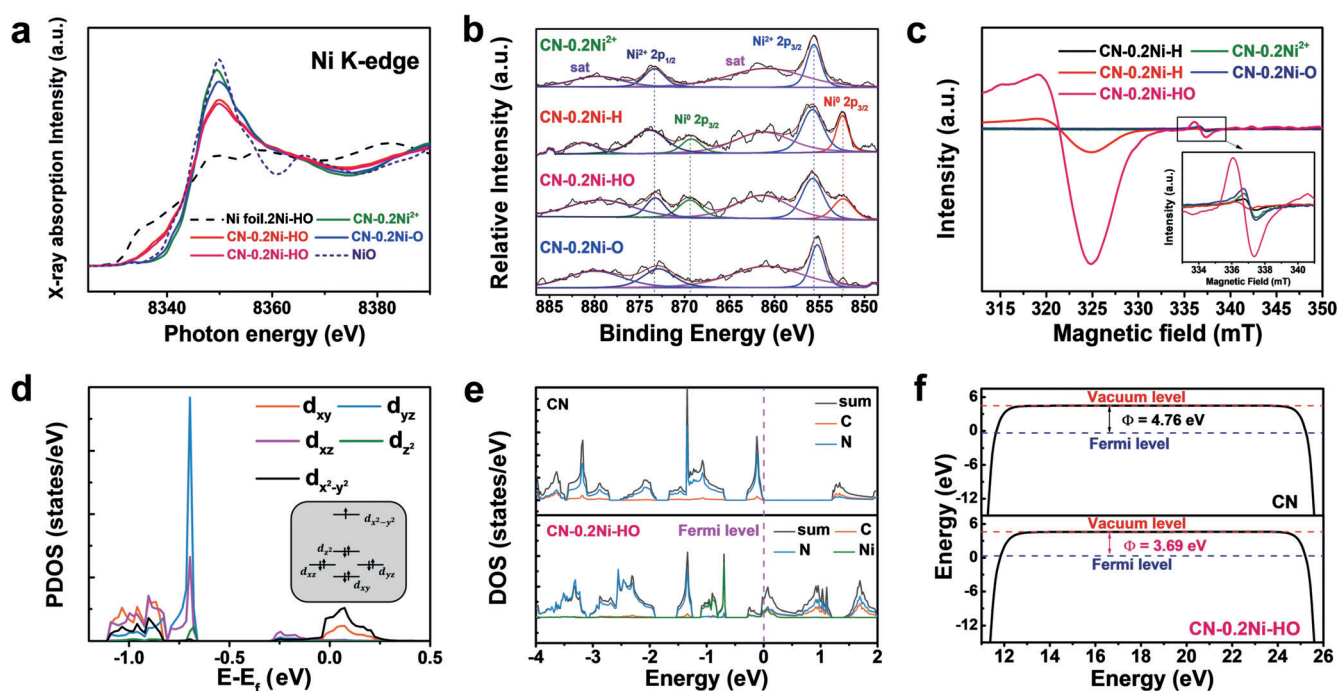


Figure 2. a) Ni K-edge XANES profiles of Ni-foil, CN-0.2Ni²⁺, CN-0.2Ni-H, CN-0.2Ni-O, CN-0.2Ni-HO, and NiO. b) High-resolution XPS Ni 2p spectra of CN-0.2Ni²⁺, CN-0.2Ni-H, CN-0.2Ni-O, and CN-0.2Ni-HO. c) EPR spectra of CN, CN-0.2Ni²⁺, CN-0.2Ni-H, CN-0.2Ni-O, and CN-0.2Ni-HO. d) Projected density of states of Ni in CN-0.2Ni-HO and energy diagram of 3d⁹ electron distribution (inset). e) Density of states of CN and CN-0.2Ni-HO. f) Work functions of CN and CN-0.2Ni-HO.

appears in CN-0.2Ni-H and CN-0.2Ni-HO, which is attributed to the unpaired electrons on Ni 3d_{x²-y²} orbital.^[9] Meanwhile, the coordination number of Ni increases with the rising chemical valence of Ni single atoms (Supporting Information, Figure S5 and Table S1). This suggests that deeply oxidized Ni single atoms are coordinated in a more saturated state than others, which thus possess less unpaired electrons comparatively (Figure 2c). The electronic configuration was further revealed by the Bader charge analysis and projected density of states (PDOS; Figure 2d; Supporting Information, Figure S6). The chemical valence of the central Ni atom was determined to be +0.73 with a 3d⁹, *S* = 1/2 electronic configuration, agreeing well with the above XANES and XPS results. As a result, the density of states (DOS) of CN has been accordingly changed (Figure 2e). The DOS of CN presents the characteristics of semiconductor in which the electrons on the valence band are donated by N atoms and no electrons are distributed around the Fermi level. Upon the introduction of Ni single-atom sites, Ni 3d electrons dominate the valence band and facilitate the conduction band crossing the Fermi level, leading to decreased band gap of the catalyst. Furthermore, the work function (3.69 eV) of Ni single-atom-coordinated CN is much lower than that of pristine CN (4.76 eV; Figure 2f), suggesting that the valence electrons in Ni single-atom-coordinated CN are apt to be excited owing to the unique 3d⁹ electronic configuration of the Ni single-atom sites. As a result, the coordination of Ni single-atom sites in CN framework has effectively elevated the visible-light response (Supporting Information, Figure S7), charge separation and migration in the photocatalyst (Supporting Information, Figures S8, S9), indicating that the partially

oxidized Ni single-atom sites are of great potentials in enhancing the photocatalytic performance of CN by modifying its electronic structure (Supporting Information, Figures S7–S9).

Photocatalytic Water-Splitting Performance

The photocatalytic performance of Ni single-atom-coordinated CN was evaluated by the water-splitting hydrogen production using triethanolamine (TEOA) as sacrificial agent (*V*_{water}:*V*_{TEOA} = 10:1). Among all the samples with different levels of Ni atomic sites, partially oxidized Ni single atoms play a decisive role in water-splitting hydrogen production (Figure 3a), agreeing well with the EPR results. The H₂ production rate reaches as high as 354.9 μmol h⁻¹ g⁻¹ at 0.2 at% of Ni single-atom content (Figure 3b), which is among the highest on the reported CN photocatalysts decorated with metal single atoms, especially cheap transition-metal single atoms (Supporting Information, Table S2). As a comparison, Ni particles of the same dosage were photo-deposited onto the surface of CN (Supporting Information, Figure S10; denoted as CN-Ni particles). It is demonstrated in Figure 3c that Ni single-atom-coordinated CN shows remarkably enhanced photocatalytic performance in comparison to pristine CN, in which the hydrogen production rate on CN-0.2Ni-HO is 36.9 and 10.1 times those on CN and CN-Ni particles, respectively. The stability of CN-0.2Ni-HO was tested by a 24 h cycling photocatalytic experiment (Figure 3d), which shows excellent catalytic performance stability with a slight rate decrease from the initial 354.9 μmol h⁻¹ g⁻¹

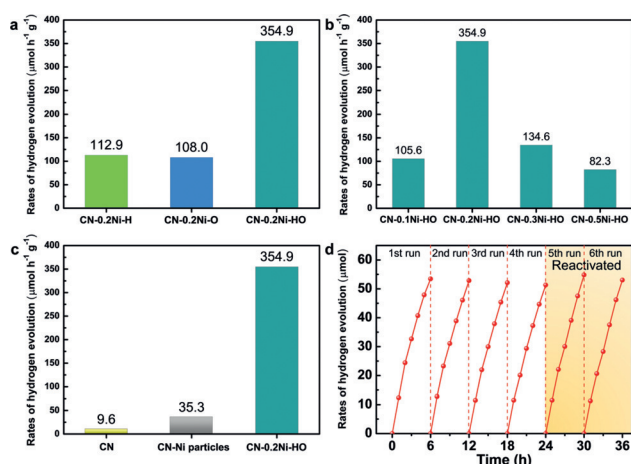


Figure 3. Photocatalytic H₂ production rates on Ni single-atom-coordinated CN catalysts a) obtained by different calcination procedures, b) with different concentrations of Ni, and c) in comparison to those of pristine CN and CN-Ni particles. d) Cycling stability of H₂ evolution on CN-0.2Ni-HO. After the 4th run, the sample was collected from the reactor, reactivated in 5% H₂/Ar and successively in 5% O₂/Ar, and put back into the same reactor for the 5th and 6th runs of photocatalytic H₂ production.

to 349.2 $\mu\text{mol h}^{-1} \text{g}^{-1}$ in 4 cycles. According to X-ray diffraction (XRD) and FT-EXAFS investigation, the surface Ni single atoms remain well-dispersed and no Ni aggregates could be identified after reaction, indicating the structural stability of Ni single atoms on CN substrate (Supporting Information, Figure S11a,b). However, XANES and XPS results reveal that Ni single atoms have been further slightly oxidized during the photocatalytic reaction (Supporting Information, Figure S11c,d). Therefore, the collected sample (denoted as After) was re-calcined in 5% H₂/Ar and successively in 5% O₂/Ar (denoted as Reactivated) to recover its originally/partially oxidized state (Supporting Information, Figure S11c,d). As a result, the photocatalytic performance was restored to 360.2 $\mu\text{mol h}^{-1} \text{g}^{-1}$ in the 5th run and stabilized

at 353.3 $\mu\text{mol h}^{-1} \text{g}^{-1}$ in the 6th run (Figure 3d). For comparison, the photocatalytic performances of CN-H and CN-O were also evaluated (Supporting Information, Figure S12), which exhibits insignificant improvements over bulky CN, indicating the negligible influences of calcination atmospheres at 350 °C on pristine CN. Taking all the above data together, we can safely conclude that the partially oxidized Ni single atoms are the actual active sites for photocatalytic H₂ evolution reaction.

Modulating the Electronic Configuration of Other Transition-Metal Single-Atom Sites

To further identify whether the valence state or the d-orbital electronic configuration is the root cause of the enhanced photocatalytic performance, control experiments were conducted on different metal species (Fe, Co, Cu). The same atomic percentage (ca. 0.2 at%) of Fe/Co/Cu single-atom sites were incorporated in CN via the same calcination treatment as Ni single-atom-coordinated CN. Their valence states and unpaired electron configurations are exhibited in the Supporting Information, Figure S13. Similar to the valence states of Ni single-atom sites, three valence states of each metal species are also observed (Supporting Information, Figure S13a–c). However, the resultant concentrations of unpaired d-electrons are quite different from that of Ni single-atom sites. As shown in the Supporting Information, Figure S13d, only Cu single-atom sites demonstrate significantly changed concentration of unpaired d-electrons during the calcination treatments. The highest concentration of unpaired d-electrons was obtained on Cu–H for Cu single atoms, different from the result of Ni single atoms, while no significant changes were found by the calcination treatments of Fe and Co single atoms. The photocatalytic H₂ production rates achieved on CN with these metal single-atom sites and metal particles are all demonstrated in Figure 4. It is clear that the photocatalytic performances achieved on the single-atom-

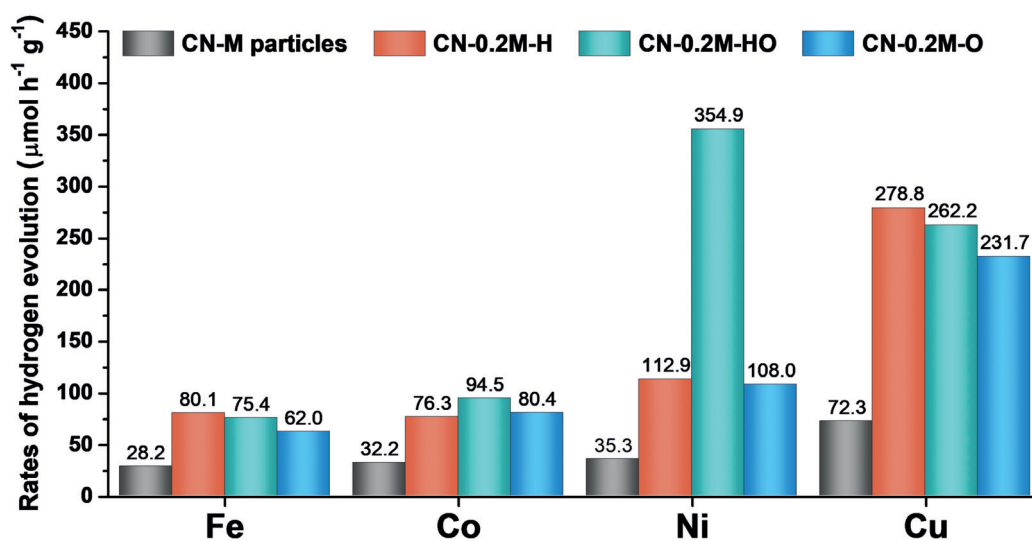


Figure 4. Photocatalytic H₂ production rates achieved on either single-atom coordinated CNs or metal nanoparticle-loaded CN. M is the metal species incorporated.

coordinated CNs are significantly improved compared to those on the corresponding metal particles-loaded CNs. More impressively, the H₂ production rates on these metal-incorporated photocatalysts are closely related to the concentration of unpaired d-electrons. Therefore, these results further show that it is the unpaired d-electrons that make the major contributions to the greatly improved photocatalytic performances.

Conclusion

We have demonstrated an effective but facile strategy to introduce nickel single-atom sites into polymeric carbon nitride (CN), and more importantly, to precisely modulate their electron configurations. Modulating the oxidation state of Ni single-atom sites into the intermediate state with a precise Ni²⁺/Ni⁰ ratio of 2 will bring the most abundant unpaired d-electrons in the photocatalyst, thus optimizing the electronic structure for remarkably enhanced photocatalytic performance. The resulting photocatalytic H₂ production rate is as high as 354.9 μmol h⁻¹ g⁻¹, which is among the highest on the reported CN photocatalysts decorated with metal single atoms, and especially cheap transition-metal single atoms. This discovery not only demonstrates the great potential of cheap transition metals as highly potential active sites, but also reveals the unique role of d-electrons of the metal single atoms in CN framework in photocatalytic reactions. Although in this work we have only modulated the electronic configuration of 3d transition metals and their activities were evaluated via simple water-splitting H₂ evolution reaction, the electronic configurations of 4d and 5d transition metals are expected also to play important roles in photo-catalyzing multiple chemical reactions, especially in modulating multi-electron-involved photocatalytic reactions, such as overall water-splitting and CO₂ reduction. This work provides a brand-new electron-level route to explore the working mechanism and enhance the performances of single-atom catalysts.

Acknowledgements

We acknowledge financial supports from the National Key R&D Program of China (2017YFE0127400), National Natural Science Foundation of China (51872317, 21835007, 21773288). We thank Ruxiang Shen from Shanghai Institute of Ceramics, Chinese Academy of Sciences for performing XPS characterization. We thank Rongfang Shen from Shanghai Institute of Applied Physics, Chinese Academy of Sciences for aiding the EPR characterization. We thank Tianjiao Xin from Shanghai Institute of Microsystem and Information Technology, Chinese Academy of Sciences for providing technical supports in morphological characterizations of Ni single-atom sites. We thank beamline BL14W1 (Shanghai Synchrotron Radiation Facility) for providing the

beam time. We thank Xiaoxia Han for helping to proof this article.

Conflict of interest

The authors declare no conflict of interest.

Keywords: electronic modulation · photocatalysis · polymeric carbon nitride · single-atom catalysts · transition metals

How to cite: *Angew. Chem. Int. Ed.* **2020**, *59*, 6827–6831
Angew. Chem. **2020**, *132*, 6894–6898

- [1] F. E. Osterloh, *Chem. Soc. Rev.* **2013**, *42*, 2294–2320.
- [2] a) B. Qiao, A. Wang, X. Yang, L. F. Allard, Z. Jiang, Y. Cui, J. Liu, J. Li, T. Zhang, *Nat. Chem.* **2011**, *3*, 634; b) X. Li, W. Bi, L. Zhang, S. Tao, W. Chu, Q. Zhang, Y. Luo, C. Wu, Y. Xie, *Adv. Mater.* **2016**, *28*, 2427–2431; c) Y. Kwon, T. Y. Kim, G. Kwon, J. Yi, H. Lee, *J. Am. Chem. Soc.* **2017**, *139*, 17694–17699; d) X. Li, X. Huang, S. Xi, S. Miao, J. Ding, W. Cai, S. Liu, X. Yang, H. Yang, J. Gao, et al., *J. Am. Chem. Soc.* **2018**, *140*, 12469–12475; e) B. H. Lee, S. Park, M. Kim, A. K. Sinha, S. C. Lee, E. Jung, W. J. Chang, K. S. Lee, J. H. Kim, S. P. Cho, et al., *Nat. Mater.* **2019**, *18*, 620–626.
- [3] a) J. Yang, D. Wang, H. Han, C. Li, *Acc. Chem. Res.* **2013**, *46*, 1900–1909; b) A. Kudo, Y. Miseki, *Chem. Soc. Rev.* **2009**, *38*, 253–278; c) J. Ran, J. Zhang, J. Yu, M. Jaroniec, S. Z. Qiao, *Chem. Soc. Rev.* **2014**, *43*, 7787–7812; d) X. F. Yang, A. Wang, B. Qiao, J. Li, J. Liu, T. Zhang, *Acc. Chem. Res.* **2013**, *46*, 1740–1748; e) X. Jin, L. Zhang, X. Fan, J. Tian, M. Wang, J. Shi, *Appl. Catal. B* **2018**, *237*, 888–894.
- [4] a) K. Jiang, S. Siahrostami, T. Zheng, Y. Hu, S. Hwang, E. Stavitski, Y. Peng, J. Dynes, M. Gangisetty, D. Su, et al., *Energy Environ. Sci.* **2018**, *11*, 893–903; b) Y. Chen, S. Ji, C. Chen, Q. Peng, D. Wang, Y. Li, *Joule* **2018**, *2*, 1242–1264.
- [5] a) H. Bin Yang, S. F. Hung, S. Liu, K. Yuan, S. Miao, L. Zhang, X. Huang, H. Y. Wang, W. Cai, R. Chen, et al., *Nat. Energy* **2018**, *3*, 140–147; b) J. Gu, C. S. Hsu, L. Bai, H. M. Chen, X. Hu, *Science* **2019**, *364*, 1091–1094.
- [6] a) Z. Y. Wu, W. B. Ji, B. C. Hu, H. W. Liang, X. X. Xu, Z. L. Yu, B. Y. Li, S. H. Yu, *Nano Energy* **2018**, *51*, 286–293; b) K. Domen, A. Kudo, T. Onishi, N. Kosugi, H. Kuroda, *J. Phys. Chem.* **1986**, *90*, 292–295.
- [7] a) X. Wang, K. Maeda, A. Thomas, K. Takanabe, G. Xin, J. M. Carlsson, K. Domen, M. Antonietti, *Nat. Mater.* **2009**, *8*, 76–80; b) Z. Chen, S. Mitchell, E. Vorobyeva, R. K. Leary, R. Hauert, T. Furnival, Q. M. Ramasse, J. M. Thomas, P. A. Midgley, D. Dontsova, et al., *Adv. Funct. Mater.* **2017**, *27*, 1605785; c) Z. Chen, E. Vorobyeva, S. Mitchell, E. Fako, N. López, S. M. Collins, R. K. Leary, P. A. Midgley, R. Hauert, J. Pérez-Ramírez, *Natl. Sci. Rev.* **2018**, *5*, 642–652.
- [8] M. Shen, L. Zhang, M. Wang, J. Tian, X. Jin, L. Guo, L. Wang, J. Shi, *J. Mater. Chem. A* **2019**, *7*, 1556–1563.
- [9] S. Xu, E. D. Walter, Z. Zhao, M. Y. Hu, X. Han, J. Z. Hu, X. Bao, *J. Phys. Chem. C* **2015**, *119*, 21219–21226.

Manuscript received: November 14, 2019

Revised manuscript received: December 30, 2019

Accepted manuscript online: January 23, 2020

Version of record online: March 9, 2020